

***On Quantifying Interfacial Thermal Resistance and Surface Energy  
during Molten Microdroplet Surface Deposition***

**D. Attinger**

Department of Mechanical Engineering , State University of New York at Stony Brook,  
Stony Brook, NY 11794-2300, USA

and

**D. Poulikakos**

Laboratory of Thermodynamics in Emerging Technologies, Institute of Energy Technology,  
Department of Mechanical and Process Engineering  
Swiss Federal Institute of Technology, ETH Center, 8092 Zurich, Switzerland.

**Abstract**

Understanding and controlling the deposition of a molten microdroplet on a colder substrate with simultaneous heat transfer and solidification is of central importance to a host of technologies, exemplified by novel methods of electronic microchip manufacturing. The physics of the involved interfacial phenomena is to date only partially understood. For instance, the transient resistance to heat transfer at the droplet-substrate interface cannot be quantified theoretically and adequate experimental data are lacking. Serious obstacles to its experimental determination are the very short time and length scales involved (of the order of microns and microseconds). In the present paper, a numerical modeling for droplet impact and solidification based on the Navier-Stokes and energy equations is used in order to reproduce transient measurements of the deposition of a eutectic Pb-Sn microdroplet on a multilayer wafer. The resistance to heat transfer at the droplet-wafer interface and the surface energy of the molten microdroplet are determined by matching numerical and experimental results. This successfully demonstrated indirect method is of interest if direct transient thermal resistance data are not available (as is very often the case).

## 1. Introduction

The fluid and heat flow phenomena occurring during the impact and solidification of a molten droplet on a flat substrate are complex. Droplet spreading is a free surface problem with large deformations in the presence of surface tension (Figure 1). An accurate determination of the droplet surface energy is important since it controls the motion of the solidifying splat, as well as the frequency of post-spreading oscillations and the final splat shape. The associated transient heat transfer and solidification processes are relevant to various novel applications [1] and involve convection in a deforming domain, complex fluid flow exemplified by the multidimensional motion of the phase change interface and the dynamics of the liquid phase, as well as conduction in the substrate [2,3]. During the spreading of a droplet on a substrate, the thermal contact between the droplet and the substrate is not perfect (due, for example, to roughness, air entrapment or substrate oxidation [4]), a phenomenon that slows down the heat transfer process.

Surface energy and heat transfer through interfaces are typical mesoscopic phenomena, whose physics is often related to nanoscale phenomena and cannot be fully understood using the classical continuum approach. A useful approach to handle these mesoscopic phenomena is to match simpler experimental measurements (of surface temperature, for example,) with simple numerical or analytical models, in order to estimate the needed parameters. Using this approach, several temperature measurements under relatively large (mm-size) solidifying droplets have been performed and matched with numerical simulations in order to estimate the values of the thermal contact resistance between the splat and the substrate [4-6]. For instance, interfacial resistance to heat transfer has been handled macroscopically and empirically by introducing a tunable contact heat transfer coefficient between the drop and the substrate [4], or by inserting a thin layer of interface of elements between the droplet and the substrate with a lower and tunable thermal conductivity [2]. In the present article, the state of the art numerical code described in [2] is used in order to reproduce transient droplet height measurements reported in [7]. The contact resistance as well as the surface tension values are the result of such comparisons.

## 2. Experiments

Results of the experimental case pertaining to this study are presented in Figure 1 and concern the impact, spreading and solidification of a molten solder droplet on a solid substrate at a lower temperature: an 80  $\mu\text{m}$  diameter  $D_0$  droplet of eutectic Pb-Sn solder at an initial temperature of 210°C impacts with a vertical velocity  $v_0$  of 1.54  $\text{ms}^{-1}$  a horizontal substrate whose initial temperature equals 48°C. The substrate is a 675  $\mu\text{m}$  thick Silicon wafer covered with layers of Au, Ti-W and Si-N, from top to bottom. The wafer and cover layer thickness and thermal

properties are described in [7] but are repeated here for completeness. The wafer consists of the following layers from top to bottom: 0.1  $\mu\text{m}$  thick Au, 0.3  $\mu\text{m}$  Ti90W alloy, 1  $\mu\text{m}$  Silicon Nitride (conductivity  $\lambda=2.33(+0.11) \text{ Wm}^{-1}\text{K}^{-1}$ , heat capacity  $\rho c_p=2.62(+0.22)*10^{-6} \text{ Jm}^{-3}\text{K}^{-1}$ , and 675  $\mu\text{m}$  P-Silicon. The substrate wafer slide is mounted on a heated copper plate with a thin layer of thermal interface paste (HTC Electrolube, England) between the wafer and the copper plate, with  $\lambda=0.84 \text{ Wm}^{-1}\text{K}^{-1}$ . The wafer top ( $T_{2,0}$ ) surface initial temperatures is measured with a K-type thermocouples (Omega 304 SS9), epoxied on the wafer with a 1mm-size island of conductive Epoxy (AV138M/HV998 Novartis, Switzerland) with  $\lambda=0.6 \text{ Wm}^{-1}\text{K}^{-1}$ . The relatively low substrate initial temperature induces solidification at the very early stages of the spreading [Ref. 3, and Figure 1], thereby reducing the influence of wetting phenomena, whose physics for impact at intermediate Weber numbers is still poorly understood [8]. Molten droplets were generated with a drop-on-demand microdroplet jetting device from MicroFab Technologies Inc. (Dallas, Texas) based on the piezoelectric generation of pressure waves in a capillary tube [1]. The technique used for the visualization of droplet impact and solidification is a strobe microscopy technique, with time and space resolution of respectively 5  $\mu\text{s}$  and 1.2  $\mu\text{m}$  [3]. Sample pictures of this visualization are shown in Figure 1.

### 3. Numerical Model

The numerical model, extensively described in [2], is formulated to simulate the impact and solidification of an initially spherical molten droplet on a flat substrate beginning at the instant of contact. The initial conditions are the same as in the experiment presented above. The model is based on the Navier-Stokes and energy equations applied to the axisymmetric coordinate system shown in the first frame of Figure 1. Constant thermophysical properties are assumed for the fluid. The assumption of a negligible temperature dependence of the surface energy is justified in the next section. The governing equations are written using a Lagrangian approach, allowing an accurate tracking of the free surface. Nondimensionalization is performed with respect to the droplet initial diameter  $D_0$ , the impact velocity  $v_0$ , the liquid density  $\rho_L$ , and the initial pressure in the drop  $p_0$  (for the pressure terms in the momentum equation, [2, 9], not shown in this paper).

Due to lack of experimental data on dynamic wetting, the wetting force at the dynamic contact angle is neglected through this analysis. The usual Navier slip condition (without needing to specify contact angles) was employed at the contact line to remove the well known stress singularity at this location [2]. Since usually freezing occurs before wetting becomes important, this approach was proven successful [2,3,7]. Gravity, radiation and natural convection effects are proven to be negligible [2, 7]. The dimensionless numbers for the fluid dynamics are defined as follows, where the subscripts L and zero stand respectively for the liquid phase of the solder, and the initial condition. The symbols  $\mu$  and  $\sigma$  stand respectively for the dynamic viscosity, and the surface energy:

$$\text{Reynolds number} \quad Re = \frac{\rho_L D_0 v_0}{\mu} \quad (1)$$

$$\text{Weber number} \quad We = \frac{\rho_L D_0 v_0^2}{\sigma} \quad (2)$$

The energy equation for the droplet and substrate is also cast in Lagrangian form. For all practical purposes, the cooling occurs through convection in the bulk fluid and conduction to the substrate [2]. It is assumed that the phase change occurs through a sharp boundary, at equilibrium temperature, and that the densities of the solid and liquid material are the same in the fluid dynamics calculation. The phase change is modeled according to the exact specific heat method [2], where the effect of latent heat release is introduced in the computation by a local increase of the heat capacities. This approach leads to the exact integration of the capacitance terms in the finite element formulation with linear triangular elements and has shown very accurate energy conservation capabilities [2]. It is assumed that the phase change occurs through a sharp boundary, at equilibrium temperature, and that the expansion upon freezing is neglected in the fluid dynamics calculation.

During the spreading of a droplet on a substrate, the heat transfer at the interface is reduced [4]. Also, in the specific case pertaining to this study, the three thin layers at the top of the substrate have different thermal conductivities than the Silicon wafer. Therefore, the interfacial resistance to heat transfer and the effect of the three top layers has been handled macroscopically by inserting a thin layer of interface elements between the droplet and the substrate with a tunable thermal conductivity  $k_3$  [ $\text{Wm}^{-1}\text{K}^{-1}$ ], [2,7], lower than the Silicon substrate thermal conductivity. It has been shown that the value of the thermal conductivity of the interface layer depends on the imperfect thermal contact only and not on the thermal conductivities of the three top layers [7]. The dimensionless interfacial conductivity  $K_3$  ( $K_3 = k_3 k_L^{-1}$ ), where  $k_L$  is the thermal conductivity of the droplet liquid phase, is related through the contact Biot number ( $Bi = h_3 k_L^{-1} D_0$ ) to the interfacial heat transfer coefficient  $h_3$  [ $\text{Wm}^{-2}\text{K}^{-1}$ ] by the equation

$$K_3 = Bi L_3 \quad (3)$$

where  $L_3$ , the dimensionless interface thickness ( $L_3 = l_3 D_0^{-1}$ ), is based on the total thickness  $l_3 = 1.4 \mu\text{m}$  of the three top layers of the substrate. Physically, this equation implies unidirectional conduction in the interfacial layer and defines an interfacial heat transfer coefficient. Our results will be expressed in terms of the contact Biot number, which is the relevant dimensionless number for interfacial conductance (inverse resistance). The heat capacity of the interface layer is determined by a weighted average of the heat capacities of the three top layers [7].

### ***Temperature dependence of the surface energy and Marangoni convection***

The temperature dependence of the surface energy is neglected in this study, i.e. the surface energy is assumed to be constant. This can be justified to some average extent by considering the effects of surface energy variation due to the cooling of the droplet, spreading on a colder surface. It has been shown in [7,10] based on an approximate analysis that, during droplet spreading on a colder substrate, the variation of surface energy due to cooling has no influence on the maximum spreading diameter if the following criterion is respected:

$$Ma \ll \frac{3Re}{2We} \quad (4)$$

The Marangoni number  $Ma$ , related to thermocapillary phenomena, is defined as follows:

$$Ma = \frac{-a(T_{1,0} - T_{2,0})}{\nu_0 \mu} \quad (5)$$

Subscripts 1,2 and 0 stand respectively for the droplet, the substrate and the initial condition. The symbol  $a$  is the temperature coefficient of the surface energy. Its value for eutectic tin-lead solder is  $-0.214 \cdot 10^{-3} \text{ [Jm}^{-2}\text{K}^{-1}]$  [11]. Using this value and the values of other needed parameters reported in the subsequent section 4, we can easily show that criterion (4) is respected: The values of the right and left hand sides are, respectively, 3.4 and 188. Therefore, the temperature dependence of the surface energy does not influence spreading, at least the maximum spreading diameter. However, another effect of the droplet surface cooling during spreading on a colder surface is the appearance of a surface energy gradient along the drop free surface. This gradient induces a fluid flow along the interface, from low to high surface energy domain. This effect, called Marangoni convection, has been neglected in this study, primarily aiming at extracting average interfacial heat transfer coefficient values by comparing simulations and experiments.

#### **4. Comparison of Numerical Simulations with Experiments**

We have performed seven numerical simulations with the code presented in [2,7] aiming at reproducing the experimental case described above and at testing the modeling sensitivity to variations of parameters like surface energy and interfacial heat transfer coefficient, represented respectively by the Weber and Biot numbers. The numerical simulation procedure is explained in [2]. A detailed study has been performed in order to obtain a solution independent of grid size and time step [7].

## Baseline Case and Parametric Variations

The simulation that was found to have the best agreement with the experiments has been performed with the following values for the thermophysical properties of the eutectic solder ( $c$ ,  $L$  and  $T_M$  are respectively the specific heat, latent heat of fusion and melting temperature):  $\sigma=0.507\text{Jm}^{-2}$ ,  $\mu=0.00262\text{Pas}$ ,  $\rho_L=8218\text{kgm}^{-3}$ ,  $\rho_S=8420\text{kgm}^{-3}$ ,  $L=42000\text{Jkg}^{-1}$ ,  $c_L=238\text{Jkg}^{-1}\text{K}^{-1}$ ,  $c_S=176\text{Jkg}^{-1}\text{K}^{-1}$ ,  $k_L=25\text{Wm}^{-1}\text{K}^{-1}$ ,  $k_S=48\text{Wm}^{-1}\text{K}^{-1}$ , and  $T_M=183\text{ }^\circ\text{C}$ . It is worth recalling that due to the small difference in the densities of liquid and solid phases, the slight expansion upon freezing was neglected in the numerical simulations. These properties and the initial conditions correspond to the experimental case described above. The following dimensionless numbers are obtained:  $\text{Re}=386$ ,  $\text{We}=3.08$ ,  $\text{Pr}=0.025$ , and  $\text{Ste}=0.765$ . The Stefan and Prandtl numbers are defined as:

$$\text{Ste}=c_L(T_M-T_{2,0})L^{-1}, \quad \text{Pr}=\mu c_L k_L^{-1} \quad (6,7)$$

The substrate is flat with radial and axial dimensions respectively four and eight times larger than the diameter of the droplet, in order to simulate the impact on a substrate much larger than the droplet. We assumed two distinct values for the interfacial heat transfer coefficient  $h_3$  ( $h_3$  was set individually for every interface element in accordance with the phase of the splat material in contact with the interface element (liquid, respectively solid)):  $h_{3L}=1.31 \times 10^5\text{Wm}^{-2}\text{K}^{-1}$ ,  $h_{3S}=1.25 \times 10^4\text{Wm}^{-2}\text{K}^{-1}$ , giving the respective contact Biot numbers,  $\text{Bi}_L=0.42$  and  $\text{Bi}_S=0.04$ . This approach can be considered as a first step toward a thorough consideration of the strong time dependence of the interfacial heat transfer measurements [4]. No systematic optimization process was performed in this study for the determination of the interfacial heat transfer coefficient. A trial and error approach was followed, guided by initial values from the literature [2,3,4, 7] as a starting point.

Four runs besides the baseline case have been performed in order to address the sensitivity of the modeling to the value of the surface energy and of the interfacial Biot number  $\text{Bi}_S$  ( $\text{Bi}_L$  is kept at a constant value that sets the initiation of the freezing at the instant of the spreading arrest).

## 5. General Description of the Droplet Oscillation Process

The temporal evolution of the dimensionless height of the droplet viewed from the side,  $H_t$ , calculated numerically for the baseline case is shown in Figure 2, and is compared with the same parameter obtained experimentally [3] (one star per measurement). The experimentally observed mildly damped oscillation process is reproduced in Figure 2 by our numerical study. The increase of the oscillation frequency is related to the reduction of the liquid mass due to the freezing process by the following equation:

$$f \propto (\sigma/\rho_L V_L)^{1/2} \quad (8)$$

which shows that the frequency  $f$  of the droplet free oscillation is proportional to the square root of the ratio of the surface energy and the liquid volume remaining in the droplet [9].

A good agreement in terms of maximum amplitude and frequency of the oscillation has been obtained for the first three periods of droplet height oscillation (latter measurements are too noisy to be interpreted). The final value of the simulated droplet height also shows a very good agreement with the measurements. It is of interest to note the existence of a double maximum in the region of the first peak of Fig. 2. A detailed study explaining its existence is contained in [12]. Here, we will only mention that it is due to the disparity between the bulk motion of the fluid in the drop and wave motion in the droplet surface. In other words, while the bulk of the liquid is moving, for example, downward, a ripple traveling across the free surface can be moving upward.

### **Parametric Variations: Surface Energy and Biot number**

The effects of *surface energy* variations are exemplified by two results shown in Figure 3, corresponding to about half ( $We = 6.0$ ), respectively twice ( $We = 1.5$ ), the surface energy of the baseline case. Only the first 200  $\mu s$  have been plotted for clarity. In the  $We=6.0$  case (lower surface energy), the frequency of the oscillations of the droplet is lower than the experimental frequency (as exemplified by the time of the second minimum of the height, 150  $\mu s$ ). Such a decrease of the oscillation frequency can be explained by means of Eq. (6). In the  $We=1.5$  case (high surface energy), the frequency of the oscillations of the droplet is higher than the experimental frequency (as exemplified by the time of the first two minima of the height).

The effects of different *heat transfer coefficients* between the substrate and the solidifying splat, expressed in terms of the solid interfacial Biot number  $Bi_S$ , are shown in Figure 4. It appears that the rate of the increase in oscillation frequency during the solidification process is proportional to  $Bi_S$  (The higher the  $Bi_S$  is, the higher the rate of increase in oscillation frequency). This can be understood by considering again Eq. (6), which relates the oscillation frequency to the inverse of the liquid volume square root. Increasing the interfacial Biot number augments the heat exchange at the interface, accelerating the solidification rate. The faster diminishing liquid volume taking part in the oscillation induces therefore a larger frequency increase of the height oscillation. Since the oscillation frequencies corresponding to  $Bi_S = 0.06$  or  $0.02$  are respectively too high or too low compared to the experimental values in Figure 2, the effective interfacial Biot number has to be between the two values.

This approach that matches measured and simulated droplet oscillations in order to determine  $Bi_S$  can be considered as a viable method for determining phenomenologically the heat transfer in the presence of an interface. Contrary to matching techniques including thermocouple measurements [4-6], the method presented in this paper is

non-intrusive, therefore better suited for experiments involving microdroplets, where a classical thermocouple measurement would have the following two drawbacks. First, it would perturb the event to observe. Second, thermocouple positioning and response would be a delicate issue, considering the highly transient and local nature of the flow field and convection heat transfer [2]. However, one should keep in mind that matching techniques such as the one developed here only give a heuristic insight in the physics of interfacial heat transfer, which is typically a microscale phenomenon. According to this lack of understanding, there is no guarantee that the values obtained for the Biot number can be used generally. We expect that this rather poor understanding of interfacial heat transfer will be improved by investigating systematically topics like non-equilibrium solidification, recalescence, as well as the influence of initial temperature difference between splat substrate on the interfacial heat transfer. To this end, it is worth noting the emergence of heat transfer studies [13, 14] using discrete methods like Molecular Dynamics. These methods at the molecular level show promise to produce a physical (not only phenomenological) insight into interfacial heat transfer.

It is also interesting to mention that a situation like the baseline case considered here, where the interfacial heat transfer coefficient is larger during the spreading than during the solidification phase ( $h_{3L} = 1.31 \times 10^5 \text{ Wm}^{-2}\text{K}^{-1}$ ,  $h_{3S} = 1.25 \times 10^4 \text{ Wm}^{-2}\text{K}^{-1}$ ), has also been evidenced in the most extensive experimental study on contact resistance to date [4], where the authors attributed this fact to the following reasons: at first, when the molten material lies upon the colder substrate, one would expect good thermal contact because the fluidity of the melt allows it to ‘match’ the shape of the substrate (with the exception of small scale roughness and gas-filled gaps). In addition, the high temperature of the melt may result in good mechanical or chemical bond between the melt and the substrate. This good contact would then degrade due to thermal contraction of the splat upon solidification. Finally, it is worth stressing that the present paper presents a method for determining the interfacial heat transfer coefficient specific to the droplet impact problem. Direct comparisons with values of interfacial heat transfer coefficients in entirely different configurations (such as chill casting [15]) have little meaning.

## **6. Conclusions**

This article presents a comparison between experimental results with microdroplets and results of a numerical modeling [2] with the goal to extract additional information on the interfacial heat transfer coefficient. A good agreement between experimental and numerical results of the oscillation process of the droplet maximum height has been obtained, and the sensitivity of the modeling to values of surface energy and interfacial Biot number has been demonstrated. Such an approach that matches experimental and numerical results, by tuning unknown problem parameters whose microscale physics makes them currently difficult to attain, is a viable method for investigating

mesoscopic phenomena such as interfacial heat transfer. This method, however, does not provide a deep insight in the physics of interfacial heat transfer. Here, diverse methods at the molecular level appear promising, but are not yet developed to the extent that they could be used reliably in realistic applications.

### Nomenclature

a	temperature coefficient of surface energy [ $\text{Jm}^{-2}\text{K}^{-1}$ ]
Bi	Biot number ( $B_i = h_3k^{-1}D_0$ )
c	specific heat
D	diameter
f	frequency
h	heat transfer coefficient [ $\text{Wm}^{-2}\text{K}^{-1}$ ]
$h_t$	droplet height over the substrate
$H_t$	dimensionless droplet height [ $H_t = h_t/D_0$ ]
k	thermal conductivity
l	thickness
L	dimensionless thickness ( $L = l/D_0$ )
$L$	latent heat of fusion
Ma	Marangoni number [ $-a(T_{1,0} - T_{2,0})/(v_0\mu)$ ]
K	dimensionless conductivity ( $K = k k_L^{-1}$ )
p	initial pressure in the drop
Pr	Prandtl number [ $\mu c_L k_L^{-1}$ ]
Re	Reynolds number [ $\rho D_0 v_0 \mu^{-1}$ ]
Ste	Stefan number [ $c_L (T_M - T_{2,0}) L^{-1}$ ]
T	temperature
$v_0$	impact velocity
V	volume
We	Weber number [ $\rho D_0 v_0^2 \sigma^{-1}$ ]
$\mu$	dynamic viscosity
$\rho$	liquid density

$\sigma$  surface energy

Subscripts

S solid

L liquid

0 initial

1 droplet or splat

2 substrate

3 splat-substrate interface

M melting

## References

1. **Hayes, D. J., and D. B. Wallace.** 1998. Solder Jet Printing: Wafer Bumping and CSP Applications. *Chip Scale Review* **2**(4):75-80.
2. **Waldvogel, J. M., and D. Poulikakos.** 1997. Solidification Phenomena in Picoliter Size Solder Droplet Deposition on a Composite Substrate. *International Journal of Heat and Mass transfer* **40**(2):295-309.
3. **Attinger, D., Z. Zhao, and D. Poulikakos.** 2000. An Experimental Study of Molten Microdroplet Surface Deposition and Solidification: Transient Behavior and Wetting Angle Dynamics. *Journal of Heat Transfer* **122**(3):544-556.
4. **Wang, G. X., and E. F. Matthys.** 1996. Experimental Investigation of Interfacial Thermal Conductance for Molten Metal Solidification on a Substrate. *Journal of Heat Transfer* **118**:157-163.
5. **Bennett, T., and D. Poulikakos.** 1994. Heat Transfer Aspects of Splat-Quench Solidification: Modeling and Experiment. *Journal of Materials Science* **29**:2025-2039.
6. **Pasandideh-Fard, M., R. Bohla, S. Chandra, and J. Mostaghimi.** 1998. Deposition of Tin Droplets on a Steel Plate: Simulations and Experiments. *Int. J. Heat and Mass Transfer* **41**(19):2929-2945.
7. **Attinger, D.** 2001. An Investigation of Molten Microdroplet Surface Deposition: Transient Behavior, Wetting Angle Dynamics and Substrate Melting Phenomenon. Ph. D. Thesis. ETH Zurich.
8. **Blake, T. D., M. Bracke, and Y. D. Shikhmurzaev.** 1999. Experimental evidence of nonlocal hydrodynamic influence on the dynamic contact angle. *Phys. Fluids* **11**:1995-2007.
9. **Fukai, J., Z. Zhao, D. Poulikakos, C. M. Megaridis, and O. Miyatake.** 1993. Modeling of the Deformation of a Liquid Droplet Impinging upon a Flat Surface. *Physics of Fluids A* **5**:2588-2599.
10. **Attinger, D., Z. Zhao and D. Poulikakos, 1999.** Analytical Estimation of the Maximum Spreading Diameter during Impact of a Drop on a Colder Surface Including Thermocapillary and Gravitational Effects, CD-Rom proceedings, ILASS 1999 Conference, Spray Impact on Wall and Films.
11. **Carroll, M. A. and Warwick, M. E.,** 1987, "Surface-Tension of Some Sn-Pb Alloys .1. Effect of Bi, Sb, P, Ag, and Cu on 60sn-40pb Solder", *Materials Science and Technology*, **3**: 1040-1045.
12. **B. Xiong, C. M. Megaridis, D. Poulikakos and H. Hoang,** 1998. "An Investigation of Key Factors Affecting Solder Microdroplet Deposition," *Journal of Heat Transfer*, **120**: 259-270.
13. **Lukes, J. R., D. Y. Li, X.-G. Liang, and C. L. Tien.** 2000. Molecular Dynamics Study of Solid Thin-Film Thermal Conductivity. *Journal of Heat Transfer* **122**:536-543.
14. **Pan Yi, D. Poulikakos, J. Walther and G. Yadigaroglu,** 2002. "Molecular Dynamics Simulation of Vaporization of an Ultra-Thin Liquid Argon Layer on a Surface," *Intl. J. Heat and Mass Transfer*, **45**: 2087-2100.

15. **Santos, C. A., Quaresma, J.M.V. and Garcia A.**, 2001. Determination of Transient Interfacial Heat Transfer Coefficients in Chill Mold Castings, *Journal of Alloys and Compounds*, **139**: 174-186.

## FIGURES

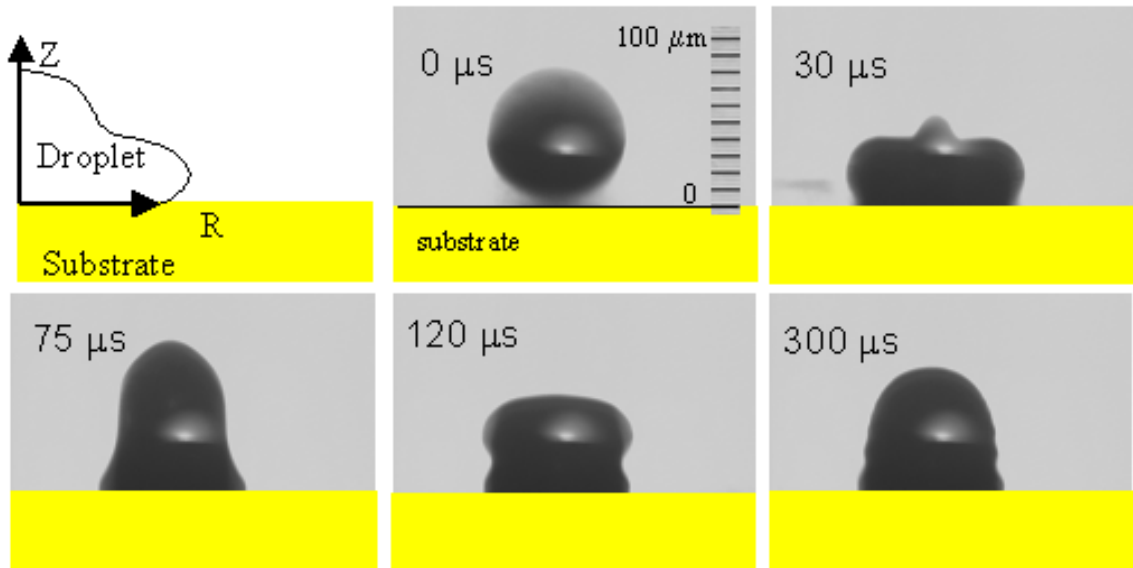


**Figure 1:** Definition of the problem to be studied. Spreading, oscillations and freezing of a solder droplet on a flat substrate from [3], with permission granted from ASME. Initial conditions:  $v_0=1.54$  m/s,  $D_0=80$  μm,  $T_{1,0}=210^\circ\text{C}$ ,  $T_{2,0}=48^\circ\text{C}$ .

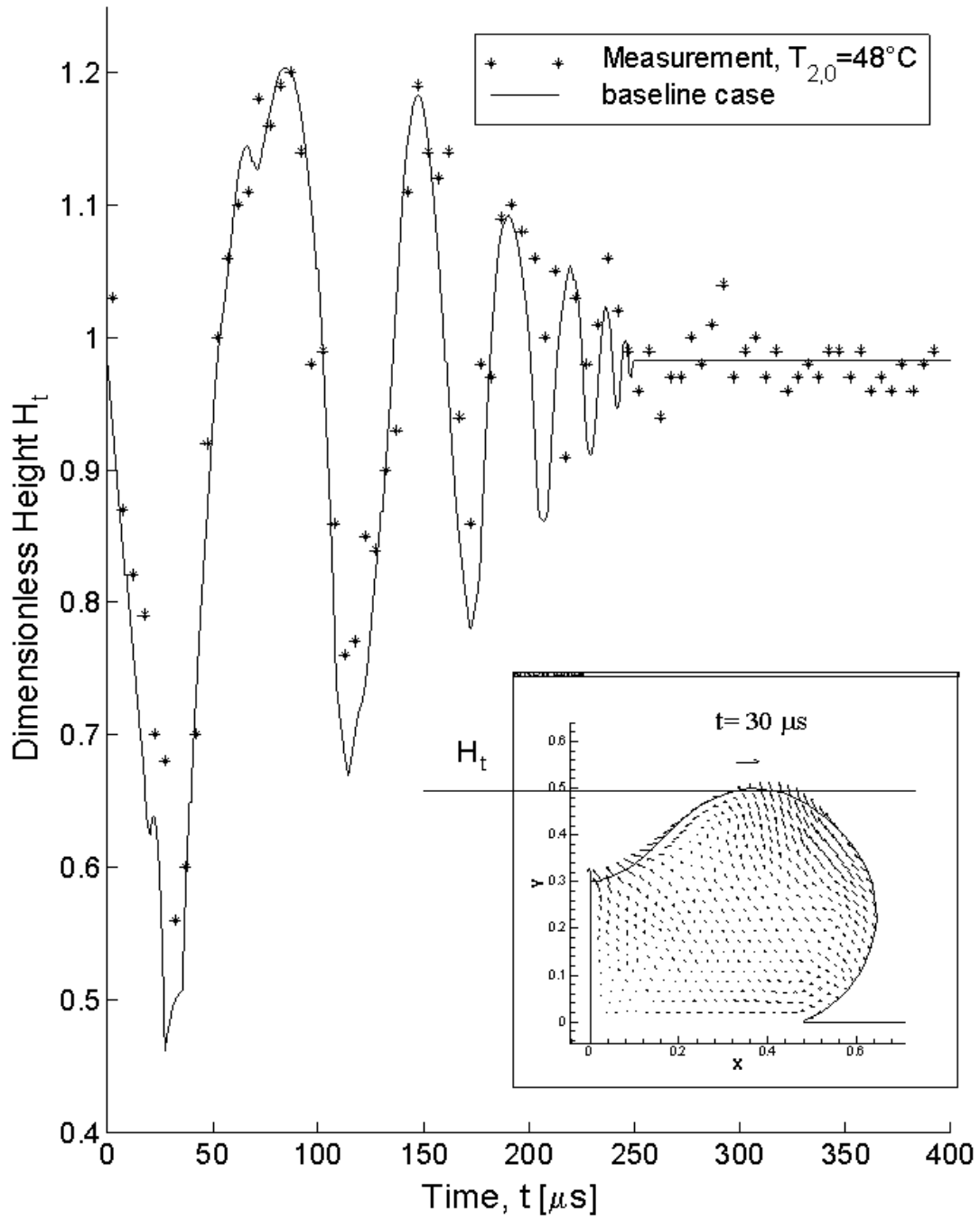


**Figure 2:** Comparison between measurement and simulation (baseline case) of the droplet height as a function of time.

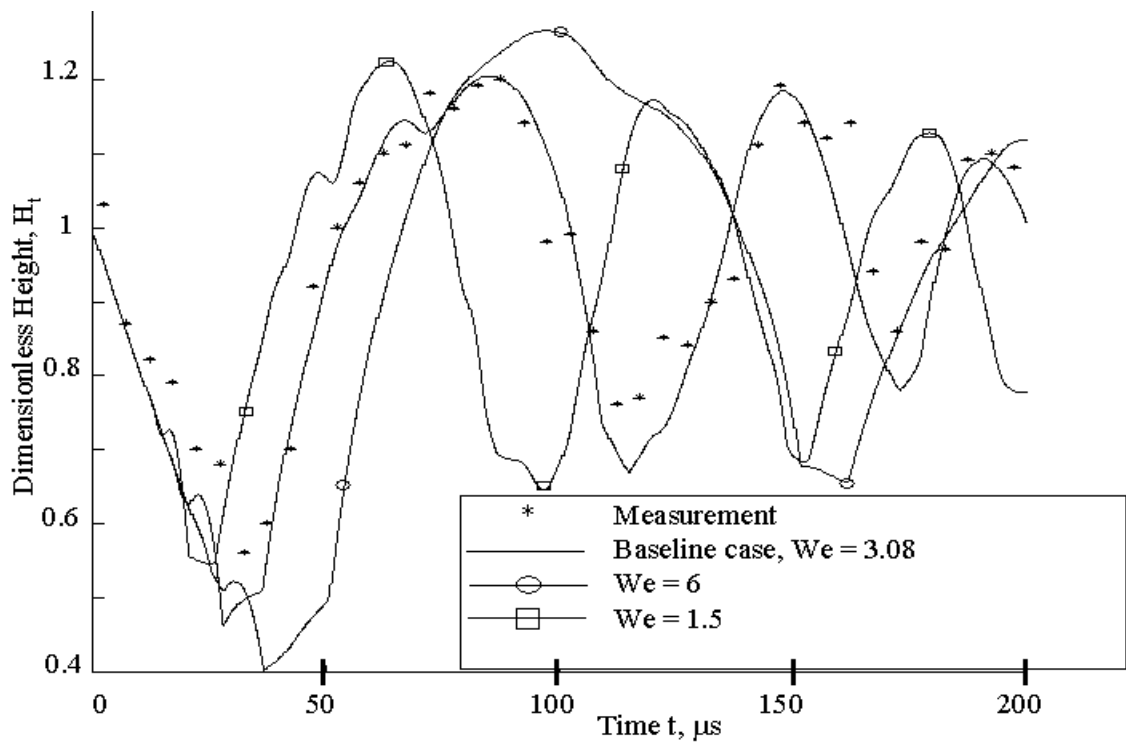


**Figure 3:** Comparison between measurement and simulations of the droplet height as a function of time, for three values of the Weber number.

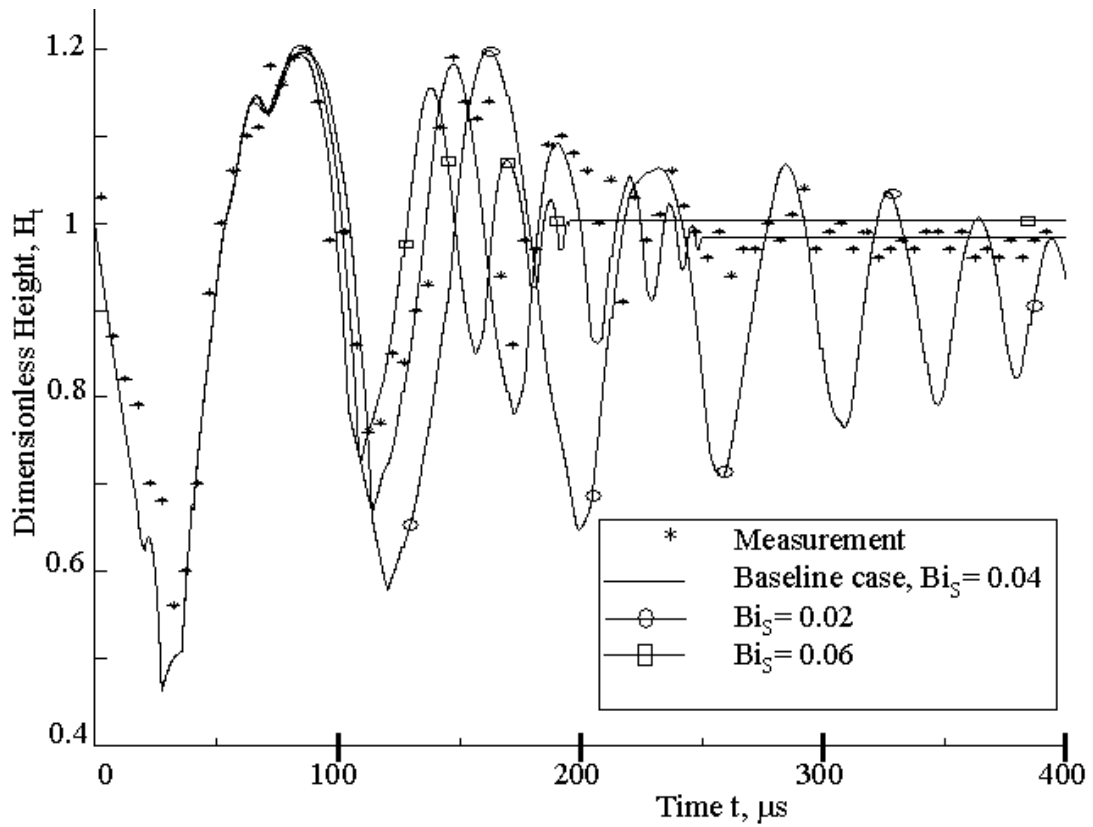


**Figure 4:** Comparison between measurement and simulations of the droplet height as a function of time, for three values of the interfacial Biot number  $Bi_s$ .